Interpretation of HRTEM images of $Sr_{0.67}Ba_{0.33}Nb_6O_2$ by simulations through the multislice approach.

Author: Sergi Plana Ruiz.
Advisor: Sònia Estradé Albiol and Lluís López Conesa.
Departament d'Electrònica, Universitat de Barcelona.

Abstract: The use of High Resolution Tranmission Electron Microscopy (HRTEM) image simulation to interpret images of complex materials has gained popularity because of the progress in the field of simulation that has taken place in the last decades. In this work, we will explain one of the methods to simulate images, the multislice approach, and we will apply it to a tetragonal tungsten bronze (TTB) material, $Sr_{0.67}Ba_{0.33}Nb_6O_2$ (SBN-67), which is an interesting material for the technology of sensors because of its electrooptical, pyroelectrical and piezoelectrical properties. Then, these simulated images will be compared to the experimental ones, acquired with a JEOL 2010F TEM, to obtain the simulated image that best fits the experimental one, as to identify which atoms are present in this structure. To simulate the images we use a C++ code provided by Earl J. Kirkland, TEMsim, which is free for download. The results of these simulations demonstrate that the multislice approach is a powerful tool to interpret TEM images in spite of the huge amount of approximations that need to be introduced.

I. INTRODUCTION

Electron microscopy is a powerful tool to acquire images and diffraction patterns with high resolution. The advantage of using electrons instead of photons is that we can obtain very small wavelengths if we apply a sufficient voltage. For instance, if we apply 10 kV to an electron, its wavelength will be 0.0122 nm and if we apply 200 kV, the corresponding wavelength will be 0.00251 nm. This means that the resolution is not determined by the particle wavelength (optical microscopes resolution is proportional to the wavelength), it is limited by the aberration of the lenses from the projector system and the alignment of the electron beam.

In High Resolution Transmission Electron Microscopy (HRTEM), images are formed due to phase contrast. The electron beam deviation due to the atomic potential of the sample can be approximated as a small change in the wavelength of the electrons as they pass through the specimen. Changing the wavelength is equivalent to shifting the phase of the electron; therefore, the electron wave function accumulates a total phase change. Because phase contrast imaging relies on differences in phase between electrons, any additional phase shifts that occur between the sample and the viewing screen can make the image impossible to interpret.

In this work, we are going to see how, using a C++ code provided by Earl J. Kirkland [1], we can simulate HRTEM images. Then, we will compare them to the experimental ones. The objective of this work is to obtain the simulated image that best fits the experimental image, in order to identify which atoms are present in the structure. It has to be said that this work is focused on the simulation of these HRTEM images, not on acquiring them. The material under study is $Sr_{0.67}Ba_{0.33}Nb_6O_2$ (SBN-67) and the comparison is performed with an image set acquired with a JEOL 2010F TEM.

II. $Sr_{1-x}Ba_xNb_2O_6$

$Sr_{1-x}Ba_xNb_2O_6$is a modulated structure which belongs to the disordered unfilled tetragonal tungsten bronze (TTB) family. The unit cell parameters are: a = b = 12.496 Å and c = 3.973 Å. Initially [2], it was suggested that this material belongs to P4bm space group but it has been seen in recent works [3] that some deviations of atomic positions from those in the centrosymmetric space group P4|mbm are highly significant but relatively small. These kinds of materials have the generalized formula $A_2B_4C_2(D_2E_8)O_{30}$ which generates three tunnel types along the z axis due to the position of Nb – O octhaedra (sites D and E) which are linked by corners: sites A, B and C. The first one, with square section, which corresponds to a 12-coordinated site, the second one, with pentagonal section, which corresponds to a 15-coordinated site, and the last one, with triangular section, which corresponds to a 9 coordinated-site. In SBN cavity A is either empty or occupied by Sr, cavity B is empty or occupied by Ba or Sr and cavity C is always empty. Furthermore, cavity B is always partially empty (this is why it is called "unfilled") and these random occupations could generate the first materialization of ferroic 3D RF Ising Model (RFIM). Another interesting fact is that the non-occupation of cavity C gives the possibility to channel electrons through it due to the absence of a strong potential which could deflect them. These configurations can be seen in Fig.(1) and Fig.(2). These big unit cell parameters and the complex phase due to the amount of atoms which forms this material makes it sensitive to the orientation and the coherence of the electron beam. This means that if the electron beam is not aligned and tilted properly, the acquired HRTEM images will not be straightforward to interpret.

The SBN wafers used in this study where grown using the Czochralski method.

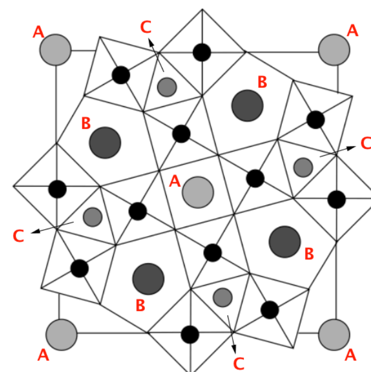

FIG. 1: Tungsten-Bronze type structure projected along c-axis.

* Electronic address: `sergiplana@hotmail.com`

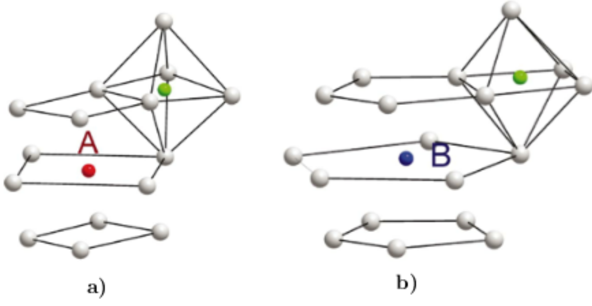

FIG. 2: a) 12-coordinated cavity in site A and b) 15-coordinated cavity in site B of a TTB structure.

This material and some doped variations have been reported as incommensurate structures (using de Wolff [4] formalism) which means that it is necessary to introduce more reciprocal base vectors besides the usual ones to describe the diffraction pattern correctly. In this way, we can write a diffraction vector as:

$$\vec{G} = k_1\vec{b}_1 + k_2\vec{b}_2 + \cdots + k_n\vec{b}_n \qquad (1)$$

This need to introduce more reciprocal base vector changed the view of these structures and opened a new interpretation. They can be understood as a modulation of unit cells along the whole sample not only referred to the unit cell, as a periodicity (or lack there of) of a "superlattice". For an accurate explanation see [4] and for a more divulgative understanding [5]. For SBN-67, it was suggested that it has two modulated vectors. It is proposed that the random occupation of the crystallographic sites A and B promotes structural variations which may be the cause for the structural incommensuration [6].

This material is a relaxor ferroelectric [8,9] with only one uniaxial polarization vector along c-axis which instead of presenting a polarization decreasing strongly when approaching Curie temperature, continues to decrease softly until it reaches zero polarization. Moreover, the peak of the dielectric susceptibility is much broader in its dependence on temperature than that of a conventional ferroelectric material, and, for this reason, these types of materials are used as capacitors. This width and maximum of the dielectric susceptibility in temperature depend on the frequency at which it is measured. The larger the frequency, the less the maximum dielectric susceptibility and the more the shift of the maximum peak with temperature.

As a member of the TTB family, it has a point group 4|mmm in the para-phase and 4mm in the ferro-phase; hence, the mirror plane perpendicular to the fourfold axis is lost at the phase transition. The transition point has not been clearly found and it has been suggested that the diffusivity to find it is due to the random distribution in A and B sites and the structural stress in addition to vacancies [6]. Furthermore, it has been reported that increasing the proportion of Sr to Ba shifts the phase transition temperature in the direction of lower temperatures and increases the dielectric susceptibility, enhancing the properties of the relaxor SBN [7].

To sum up, the disorder and random distribution of A and B cavities in SBN cause the appearance of nanoelectric fields pointing along c-axis and results in large pyroelectric, electrooptic and piezoelectric tensor components. This can be the reason why this material has relaxor properties and its potential application in thermoelectrical, pyroelectrical and piezoelectric devices and sensors are currently in study.

III. METHOD TO SIMULATE IMAGES

Prior to the simulations, we need to create the unit cell for the structure we want to simulate. To do so, we use a software from University of Cadiz, which allows building unit cells and supercells with a given orientation. Only the Wickoff position of each atom of the structure is needed, which can be found at the Bilbao Crystallographic Server, for example. Once the sample has been created, we are ready to consider the simulation itself.

In order to interpret the experimental images it is necessary to use models. In our case we will consider a linear image approximation in which the actual recorded image intensity, $\mathbf{g}(\mathbf{x},\mathbf{y})$, is related to the ideal image of the object, $\mathbf{f}(\mathbf{x},\mathbf{y})$, by a linear convolution of the object function with the point spread function of the objective lens, $\mathbf{h}(\mathbf{x},\mathbf{y})$, of the TEM.

$$g(x,y) = f(x,y) \otimes h(x,y) \qquad (2)$$

Using the Fourier convolution theorem the linear image model can also be written as a product in Fourier or reciprocal space. In this model we will not take into account the projector system, which magnifies the image, because when we obtain the simulated image it will be referred to the dimensions of the specimen

In an electron microscope the energy of the incident electrons (200 keV in our case) is much greater than the additional energy that they gain (or lose) inside the specimen. This means that the electron motion will be predominately in the forward z direction, along the optical axis of the microscope. Moreover, if the specimen is thin enough, the electron wave function will accumulate a total phase change while passing through the specimen that is just the integral of the potential of the specimen. In this way, the transmitted electron wave function can be described as:

$$\psi_t(x,y) = t(x,y)\psi_{inc}(x,y) \qquad (3)$$

$$t(x,y) = exp\,[i\,\sigma\,v_z(x,y)] \qquad (4)$$

where $\psi_{inc}(x,y)$ is the incident electron wave function and $v_z(x,y)$ is the projected atomic potential, which is defined as:

$$v_z(x,y) = \int V_s(x,y,z)dz \qquad (5)$$

This is called the Weak Phase Object (WPO) approximation.

This approximation is valid if we have thin samples. In order to take advantage of it, we will use the multislice approach. This approach consists in dividing the sample in slices of Δz, so the WPO approximation is valid for each individual slice. At each slice the electron wave function experiences a phase shift due to the projected atomic potential of all atoms in the slice and then it is propagated in vacuum along z for the thickness of the slice. In general, each

one is independent from all others, so both the slice thickness Δz and transmission function may vary from one to the next. In this way, we have to calculate the propagation of the wave function of the beam inside each slice of the sample with the Schrödinger equation.

$$\left[\frac{\hbar}{2m}\nabla^2 - eV(x,y,z)\right]\psi(x,y,z) = E\ \psi(x,y,z) \quad (6)$$

If we solve this equation assuming weak phase object approximation and neglecting terms greater than Δz^2, we can find the solution for each slice:

$$\psi_{n+1}(x,y) = t_n(x,y)[p_n(x,y,\Delta z) \otimes \psi_n(x,y,z)] \quad (7)$$

where the label n indicates the slice that we are referring to. $t_n(x,y)$ is the transmission function through the 2D projected potential, and $p_n(x,y,\Delta z)$ is the propagator function and it describes the propagation in vacuum in the z axis when we have the electron beam going through the specimen. The initial wave function for a TEM in partial coherent conditions is: $\psi_0(x,y) = \exp(2\pi K_\beta X)$, where $K_\beta = (k_{x_\beta}, k_{y_\beta})$ and $X = (x,y)$. β is called the illumination semi-angle , which is the angle of the incident illumination to the sample with respect to the optic axis.

Now that the electron beam has passed through the sample, the microscope has to create the image to view at the screen. To do so we have an objective system and we need a function that simulates the aberrations of the lenses that compose this system. This function is called the phase contrast transfer function, $h_0(x,y)$.

The conditions in which we have to simulate images are that: incident illumination is never exactly collimated and parallel to the optic axis of the microscope, electron energy is not completely monochromatic and objective and condenser lens currents are never perfectly stable. So, if we take into account all of these points we are in partially coherent conditions of image simulations and $h_0(x,y)$ has as parameters: the third- and fifth- order spherical aberrations coefficients (C_{s3} and C_{s5}, respectively), the defocus spread (Δ_0), which contains the fluctuations of the electron energy, lens currents and acceleration voltage, and the defocus value (Δf), which can be defined as the deviation of the defocused image plane from the ideal Gaussian image plane. In this way, the phase contrast transfer function in the reciprocal space is of the form plotted in Fig.(3). The coherent conditions assume the electron beam is completely parallel to the zone axis and monochromatic.

Ideally, a transfer function would be flat and have the same sign over the range of spatial frequencies that are transmitted to the image. The oscillatory nature can cause serious problems because it is not flat and changes sign. So, in order to avoid these problems, it is better to limit the range of spatial frequencies so that the transfer function at least has the same sign over its allowed range. To do so, an objective aperture is placed in the back focal plane of the objective lens and the radius of this aperture cuts the transfer function as needed. This aperture limits the number of deflected beams up to a maximum angle, α, the objective angle.

Finally, we have all the mathematical representations for the electron wavefunction propagating along the TEM column. Therefore, the image that we will obtain can be described as:

$$g(x,y) = |\psi_t(x,y) \otimes h_0(x,y)|^2 \quad (8)$$

Now we are ready to simulate the images and compare them with the experimental ones.

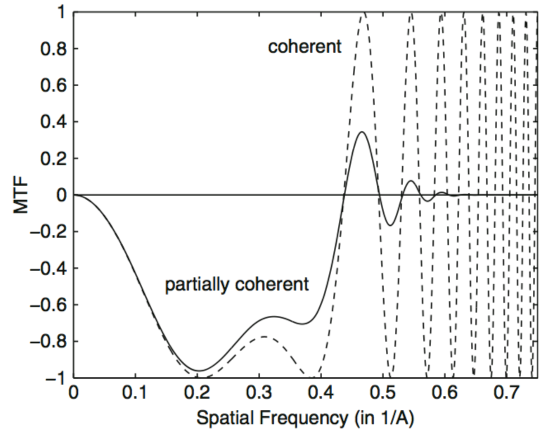

FIG. 3: The modulated transfer function or phase contrast transfer function with and without partial coherence conditions, with respect to the spatial frequency. The variables used are $C_{s3} = 1$ mm, $C_{s5} = 0$, $\Delta_0 = 100$ Å, $\beta = 0.5$ mrad, $E = 200$ keV and $\Delta f = 630$ nm.

IV. RESULTS

First of all, we present in Fig.(4) the image obtained with a JEOL 2010F, a field emission TEM, in High Resolution with [001] as a zone axis and after having applied some filters to the Fourier transform in order to have a more understandable and useful image to begin with.

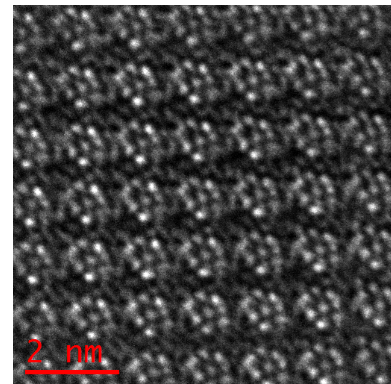

FIG. 4: [001] SBN HRTEM image obtained with a JEOL 2010F TEM with 1M of magnification.

Upon close examination of this image, it is apparent that the sample is tilted with tilt axis in a direction from lower right side to upper left side (NW direction). The reason why each unit cell has a flower-like shape instead of a homogenous mix of spots is not straightforward. It looks like the electron beam is attracted around one of the B sites. Beam conditions and column alignment can produce some distortions at high magnifications and could be the reason for this.

First of all we create the sample model. The specimen that we use to simulate all the images, is created with the

University of Cadiz (UCA) software and it has a size of $62.5 \times 62.5 \times 19.89$ Å^3 because we want to have 5 unit cells in the surface dimension and a sample thickness of approximately 20 nm. (Accordingly to the measures of low loss Electron Energy Loss Spectroscopy, the sample has this thickness) in order to compare with Fig. 3. However, changing the thickness in 5 nm. or 10 nm. does not change appreciably the resolution of the image. Also, we impose z-axis parallel to [001] crystallographic direction and y-axis parallel to [100]. At the moment we will not introduce any tilt to the sample and we will use $\Delta z = 2$ Å.

The first step is to simulate the structure with ideal conditions. This means that we will impose the defocus spread and the spherical aberrations to be zero. In these conditions, we acquire a set of images varying the defocus value and the objective aperture size. For each objective aperture size, we have to find the best defocus value that gives more resolution to the image. For this reason, depending on this aperture, we will find different defocus values. Another interesting thing is that if we increase the aperture size we will gain resolution. This is so because we are taking into account more interplanar distances. Also, it has to be noticed that if we continue increasing this parameter we will reach the zero transfer function and, after this point, it can happen that other smaller distance planes invert the sign value of the transfer function causing a reduction of the image contrast. In this way, we find that the best objective aperture size is 18 mrad; the corresponding image is given in Fig.(5).

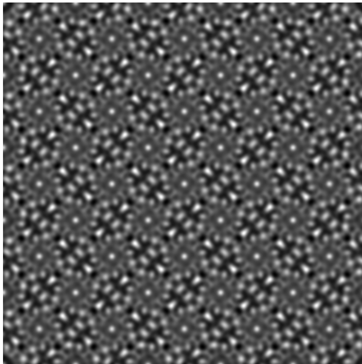

FIG. 5: Simulated image of SBN [001] with $C_{s3} = C_{s5} = 0$, $\Delta_0 = 0$, $\beta = 0.7$ mrad, α = 18 mrad and $\Delta f = 320$ nm.

If we pay attention to this last figure we realise that it is not very similar to the experimental one. This is because we are not taking into account the experimental conditions of the JEOL 2010F. For this microscope, $C_{s3} = 0.5$ mm, $C_{s5} = 0$ (it is not exactly 0 but it is negligible with respect to C_{s3}) and $\Delta_0 = 50$ Å. Applying an objective aperture angle set between 12 to 18 mrad and making an image sweep changing the defocus, we find the best image (with $\Delta f = 630$ nm), which is presented in Fig. (7).

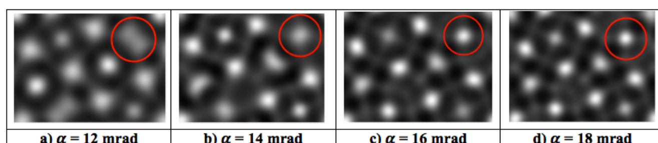

FIG. 6: Zoom from the simulated image of SBN [001] with $C_{s3} = 0.5$ mm, $C_{s5} = 0$, $\Delta_0 = 50$ Å, $\beta = 0.7$ mrad and $\Delta f = 630$ nm for different objective aperture angles.

In this last set of images we can see again an increase of resolution with objective aperture size. A clarifying example of that is given in Fig.(6), in which a point that apparently seems to correspond two atoms and can not be differentiate at 12 mrad, turns out to be one simple point at 18 mrad.

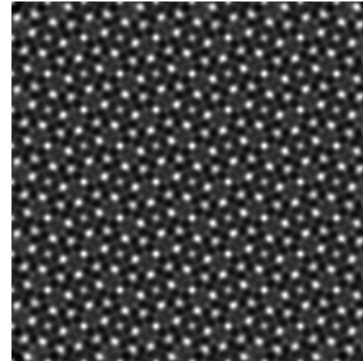

FIG. 7: Simulated image of SBN [001] with $C_{s3} = 0.5$ mm, $C_{s5} = 0$, $\Delta_0 = 50$ Å, $\beta = 0.7$ mrad, α = 18 mrad and $\Delta f = 630$ nm.

Now, we have something that we can compare to the experimental image but we have to introduce a tilt to the sample in the NW direction to consider some orientation deviations from the zone axis. To do so, UCA server provides an option to tilt the sample with respect to the x, y or z axis in degrees. In order to obtain a NW axis tilt direction we have to apply a negative rotation with respect to x-axis (R_x) and a positive rotation with respect to y-axis (R_y) (Or to apply the same rotations but with reverse sign ($R_x > 0$ and $R_y < 0$)). Because the image results and the method is equivalent, a swept of tilt values is performed with respect to x-axis between -5º and 0º and with respect to y-axis between 0º and 5º increasing one degree in each simulation. So, we have 35 tilt combinations with a range of defocus values each one as well, to choose the one with best contrast and resolution. Some of these tilted sample simulated images can be see in Fig.(8).

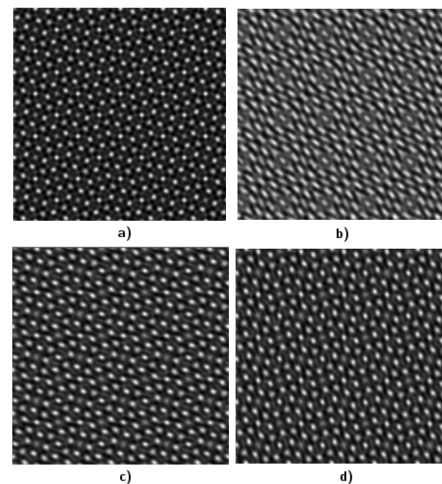

FIG. 8: Simulated images of SBN with a) $R_x = -1^{\circ}$ and $R_y = 1^{\circ}$, b) $R_x = -5^{\circ}$ and $R_y = 5^{\circ}$, c) $R_x = -2^{\circ}$ and $R_y = 4^{\circ}$ and d) $R_x = -4^{\circ}$ and $R_y = 2^{\circ}$. The conditions used are $C_{s3} = 0.5$ mm $C_{s5} = 0$, $\Delta_0 = 50$ Å, $\beta = 0.7$ mrad, α = 18 mrad and $\Delta f = 670$ nm.

After that, and knowing that the best simulated image is between 1 and 3 degrees at both axes from the observation of

the 35 tilt combinations, we try from $R_x = -1^{\circ}$ and $R_y = 3^{\circ}$ to $R_x = -3^{\circ}$ and $R_y = 1^{\circ}$ proportionally subtracting 0.1º in both rotations in each step, hence, 18 more different tilt combinations. The result of this procedure does not change the image appreciably. The final simulated image that fits best the experimental one is given in Fig.(9).

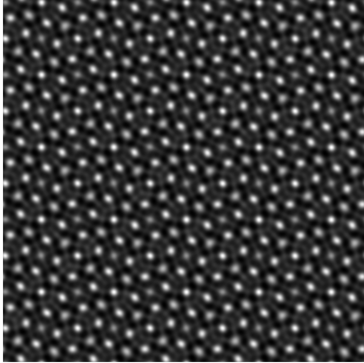

FIG 9. Simulated image of SBN tilted -2º with respect to x-axis and 2º with respect to y-axis. The conditions used are $C_{s3} = 0.5$ mm $C_{s5} = 0$, Δ_0= 50 Å, $\beta = 0.7$ mrad, α = 18 mrad and $\Delta f = 660$ nm.

With this simulated image we are prepared to identify the atoms from the experimental image. To do this we find the flower shape in the simulated image and with the help of the atomic model we can identify the atoms. This procedure is shown in Fig.(10).

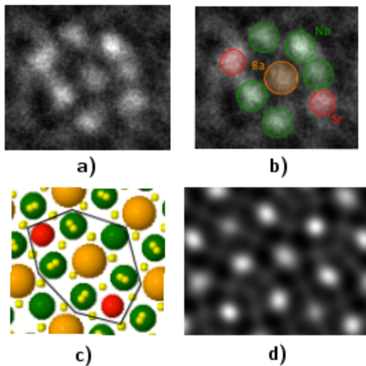

FIG 10. a) Real SBN zoom from Fig. 4, b) the same image with indications of the atoms/sites, c) the atomic model from UCA server and d) the same zone of the simulated image.

As we can see in Fig.(10), there are some displacements for the Niobium and Strontium atoms at the lower right side compared with the unit cell of the SBN structure. This can be due to a drift at the moment of acquisition or some objective astigmatism as well. However, it is quite clear that these zones correspond to the proposed sites.

V. CONCLUSIONS

- In this work, we are able to identify the atomic sites in an experimental HRTEM image of SBN-67 applying the multislice approach to simulate it. Although it requires a huge amount of images with several variations of parameters to find the one that fits better the experimental image, it is a powerful tool to interpret HRTEM data.
- The main problem of these simulations is that it takes a long time to find the best simulated image to compare with the experimental one. For this reason, it would be interesting to create a bash code that reproduces the steps we have followed in this work. To do so, the code should make a sweep in the objective aperture, tilt of the sample and defocus (in this order) and use the experimental conditions of the microscope. Each simulated image should be compared to the experimental one and, finally, the image that better fits the experimental one and its related simulated parameters should be displayed. However, it is not straightforward to find the optimum algorithm to compare the simulated images with the experimental one due to the changing acquisition conditions of the latter.

Acknowledgments

I would like to thank Sònia Estradé and Lluís López from the Electronics department of UB for their patience to explain and correct my mistakes through the training of the simulations as well as the support from the transmission electron microscopy unit from CCiT-UB. I also want to thank my parents for encouraging me at the stressful moments.

[1] Kirkland, E. J. (2010). Advanced Computing in Electron Microscopy 2nd Edition.

[2] Jamieson, P. B., Abrahams, S. C. and Bernstein, J. L. (1968). J. Chem. Phys. 48, 5048-5057.

[3] D. Schaniel, J. Schefer, B. Delley, M. Imlau, and Th. Woike. (2002). Phys. Rev. B 66, 085103.

[4] Wolff, P. M. de. (1974). Acta Cryst. A30, 777-785.

[5] Chapuis G. and Arakcheeva a. (2013). Infoscience, 1720-0776.

[6] E. Martínez, A. Fundora, H. Amorín, J. Portelles and J. M. Siqueiros. (2002). J. Appl. Phys. 91, 3154.

[7] Anatolii Belous, Oleg V'yunove, Dmitrii Mishchuk, Stanislav Kamba and Dmitry Nuzhnyy. (2007). J. Appl. Phys. 102, 014111.

[8] G. G. Guzmán-Verri, C. M. Varma. (2012). arXiv:1212.3402.

[9] R. A. Cowley, S. N. Gvasaliya, S. G. Lushnikov, B. Roessli and G. M. Rotaru. (2011). Adv. Phys. 60, 229.

[10] Williams D. B., Carter C.B. (2009). Transmission Electron Microscopy 2nd Edition.